

MERGER SHOCKS IN GALAXY CLUSTERS A665 AND A2163 AND THEIR RELATION TO RADIO HALOS

M. MARKEVITCH AND A. VIKHЛИNIN¹

Harvard-Smithsonian Center for Astrophysics, 60 Garden St., Cambridge, MA 02138; maxim, alexey @head-cfa.harvard.edu

Submitted to ApJ

ABSTRACT

We present *Chandra* gas temperature maps for two hot, intermediate-redshift clusters A665 and A2163. Both show strong temperature variations in their central $r = 0.5 h^{-1}$ Mpc regions, naturally interpreted as product of the subcluster mergers. The A665 map reveals a shock in front of the cool core, while the temperature structure of A2163 is more complicated. On a larger linear scale, our data on A2163 indicate a radial temperature decline in agreement with earlier *ASCA* results, although the uncertainties are large. Both these clusters exhibit previously known synchrotron radio halos. Comparison of the radio images and the gas temperature maps indicates that radio emission predominantly comes from the hot gas regions, providing a strong argument in favor of the hypothesis that relativistic electrons are accelerated in merger shocks.

Subject headings: Galaxies: clusters: individual (A665, A2163) — intergalactic medium — radio continuum: galaxies — acceleration of particles

1. INTRODUCTION

The intracluster medium (ICM) is heated to the observed high temperatures by gas-dynamic shocks when the cluster is formed through infall and merging of smaller subunits. In clusters currently undergoing mergers, such shocks may be identified in the gas temperature and density maps, if the geometry of the merger is favorable. The ICM density and temperature can be derived from X-ray data. Due to the difficulty of the spatially-resolved X-ray spectroscopy, so far only a few nearby clusters have been studied in sufficient detail, but a number of them indeed exhibit the characteristic irregular temperature structure (*ROSAT* and *ASCA* results, e.g., Henry & Briel 1995; Markevitch, Sarazin & Vikhlinin 1999 and references therein; *Chandra* and *XMM* results, e.g., Markevitch et al. 2000; Vikhlinin, Markevitch, & Murray 2001; Neumann et al. 2001).

At radio frequencies, some clusters exhibit large, centrally located, low surface brightness halos with relatively steep spectra (for historic references see, e.g., Sarazin 1988; recent works, e.g., Giovannini, Tordi, & Feretti 1999 and references therein). Such halos are relatively rare. They are generated by a population of ultra-relativistic electrons (coexisting with thermal electrons of the ICM) that emit synchrotron radiation in the cluster magnetic field. Such electrons should be relatively short-lived ($\sim 10^8$ yr) due to inverse Compton and synchrotron energy losses, and yet they must have time to spread over the cluster volume or they should be accelerated in situ. The source of such electrons that can support a halo for a sufficient time is unclear. Several possibilities were proposed, including radio galaxies (Jaffe 1977), interaction of cosmic ray protons with the ICM protons (Dolag & Enßlin 2000 and references therein), and the turbulence generated by merger shocks (Harris, Kapahi, & Ekers 1980; Tribble 1993). Indeed, merger shocks dissipate vast amounts of kinetic energy that, besides heating the intracluster gas, may power the amplification of magnetic fields and acceleration (or re-acceleration) of relativistic particles. A correlation between the existence of a radio halo and

the irregular cluster shape (that usually indicates a merger) has been noticed (e.g., Feretti 2000 and references therein; Buote 2001) and seems to favor the latter mechanism. However, as pointed out by Liang et al. (2000), this correlation may be a selection effect arising from the technical difficulty of detecting low surface brightness halos in relaxed clusters that usually have strong central radio sources. It was also noticed for several well-resolved halos that the radio brightness follows the X-ray brightness on large scales (e.g., Deiss et al. 1997; Govoni et al. 2001). Obviously, the best check of the significance of merger shocks for the radio halo formation would be to find the shocks and see if there is any relation between their location and the radio emission.

In this paper, we analyze short *Chandra* ACIS observations of two hot clusters A665 ($z = 0.182$) and A2163 ($z = 0.201$). Their structure was studied with earlier X-ray telescopes, most recently with *ROSAT* (e.g., Buote & Tsai 1996; Gómez, Hughes, & Birkhaw 2000; Elbaz, Arnaud, & Böhringer 1995), and the crude temperature maps were derived with *ASCA* (Markevitch et al. 1994; Markevitch 1996). Those data suggested that both clusters are undergoing mergers. Using the new ACIS data, we derive the gas temperature maps at a much finer linear scale and locate the sites of shock heating of the ICM. Both these clusters have giant radio halos (discovered in A665 by Moffet & Birkhaw 1989 and in A2163 by Herbig & Birkhaw 1994). For the first time for any radio halo clusters, we compare the radio images and the gas temperature maps. We use $H_0 = 100 h \text{ km s}^{-1} \text{ Mpc}^{-1}$ and $\Omega_0 = 0.3$; confidence intervals are one-parameter 90%.

2. DATA ANALYSIS

A665 was observed on 1999 December 29 with ACIS-I² using chips I0–I3 and S2. The useful exposure was 8550 s; there were no background flares (Markevitch 2001) during the observation. A2163 was observed on 2000 July 29 using the same ACIS configuration. The useful exposure was 9560 s and there were no background flares. Events with bad grades and those

¹Also Space Research Institute, Russian Academy of Sciences²*Chandra* Observatory Guide <http://asc.harvard.edu/udocs/docs/>, “Observatory Guide”, “ACIS”

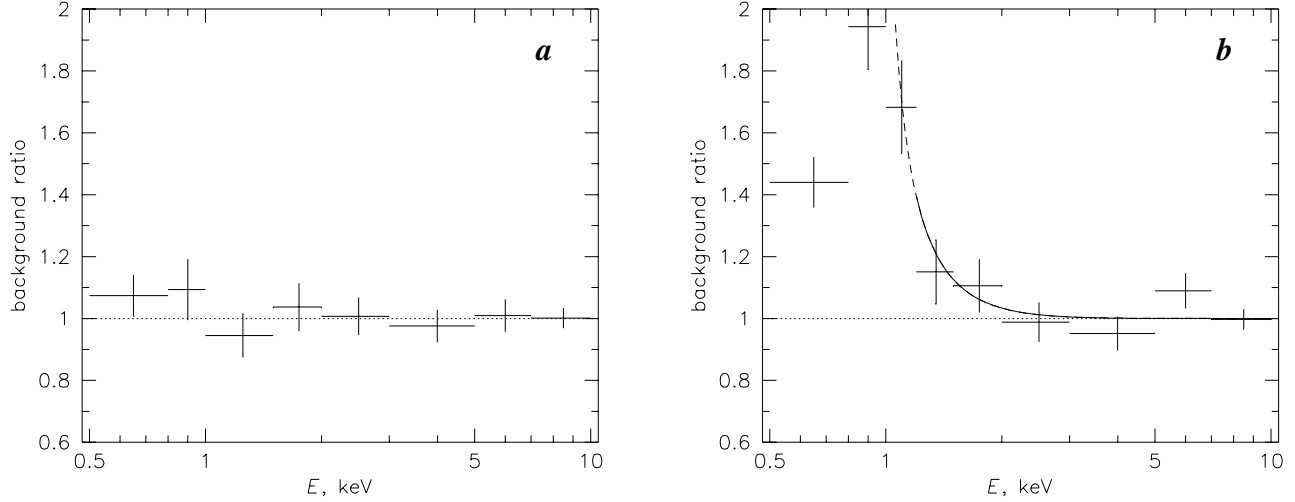


FIG. 1.—Ratio of the observed background rate in chip S2 (that has negligible cluster emission) to the expected rate from the blank-field data corrected for a long-term trend, (a) for A665 and (b) for A2163. Vertical errors are 1σ . For A2163, an approximate analytic description of the ratio is shown (the line is solid in the $E > 1.2$ keV interval that is used for spectral fits). This soft excess can also be described by a thermal emission arising from a warm foreground gas (our preferred method, see text).

originating from bad pixels and columns were screened out in a standard manner.

2.1. Background subtraction

Background subtraction is critical for deriving the temperatures in the low-brightness regions at high cluster radii, which is one of the goals of this work. The main component of the background is modeled using the composite blank-field datasets³ for the corresponding focal plane temperature, normalizing them by the ratio of the exposures and a small energy-independent correction factor that reflects the long-term decrease of the background (0.95 for A665 and 0.93 for A2163, determined by the observation dates). The background datasets include mostly the fields with low Galactic N_H , appropriate for most clusters including A665. However, A2163 has a relatively high N_H (there is also an unusual difference between the Galactic HI measurements and the best-fit *ROSAT* PSPC value, see Elbaz et al. 1995), thus we should verify the applicability of the standard background. In both observations, we can compare the background model to the data from chip S2 that covers a region sufficiently far from the cluster centers to ignore the cluster contribution. Figure 1 shows the ratios of the spectra from chip S2 to the spectra from the respective blank field datasets with proper normalizations. For A665, the model predicts the observed S2 background perfectly.

The A2163 observation, however, shows a clear soft excess, already noticed by Pratt et al. (2001) in the *XMM* observation of this cluster. This excess may be due to the local enhancement of the diffuse Galactic background, or a temporary increase of the soft particle background at the time of the observation, or a combination thereof. An excess is also seen in the *ROSAT* PSPC observation of this field, thus, given all the data, a genuine enhancement in the sky is more likely. Examination of the *ROSAT* PSPC image in the relevant 0.7–1.3 keV band shows no spatial variations of the soft background in the vicinity of A2163 to within 5%. Therefore, we can model this excess by fitting its spectrum from chip S2 and then adding the best-fit

model, scaled by the region area, to the model of the cluster emission (thus a small difference in vignetting between the cluster position and the field covered by S2 will be taken into account properly). After the subtraction of the nominal blank-field background, the S2 excess spectrum in the 0.5–3 keV band is described quite well by a simple absorbed thermal model (MEKAL, Kaastra 1992) with $T = 0.3$ keV, $z = 0$, a metal abundance unconstrained but consistent with solar, and the absorption column consistent with the *ROSAT* PSPC value derived by Elbaz et al. (1995) for this cluster. The observed surface brightness of the soft excess is 2×10^{-15} erg s⁻¹ cm⁻² arcmin⁻¹ in the 0.5–1 keV band, within a factor of 2 of the approximate *ROSAT* PSPC estimate.

On the other hand, if the observed excess is due to the temporary increase of the particle background, it would not be vigneted in the same way as are X-rays from the sky. If so, a better approach would be to fit a correction function to the spectral ratio in Fig. 1b and multiply by it the nominal background model for the cluster regions. Such a function is shown in Fig. 1b for the energy band of interest. We tried both methods of the soft excess correction and found the results almost identical, thus the physical nature of this component is unimportant for the purposes of this paper. We will use the spectral modeling method below.

When deriving the A2163 temperature profile (§2.4), we tried to minimize the influence of the soft background excess by discarding the data with $E < 1.2$ keV where the excess is greater than 50% of the nominal background (Fig. 1b), and in the remaining energy band, using the warm gas model derived above. The 1.2 keV energy cutoff is used for all A2163 radial bins for uniformity. Using a still higher cutoff would further limit the background uncertainty but also decrease the statistical accuracy of the results.

The ACIS readout artifact, although not particularly important in the absence of sharp brightness peaks in these clusters, was subtracted as an additional background component. It was modeled under the assumption of no pile-up by randomizing

³Described at <http://hea-www.harvard.edu/~maxim/axaf/acisbg>

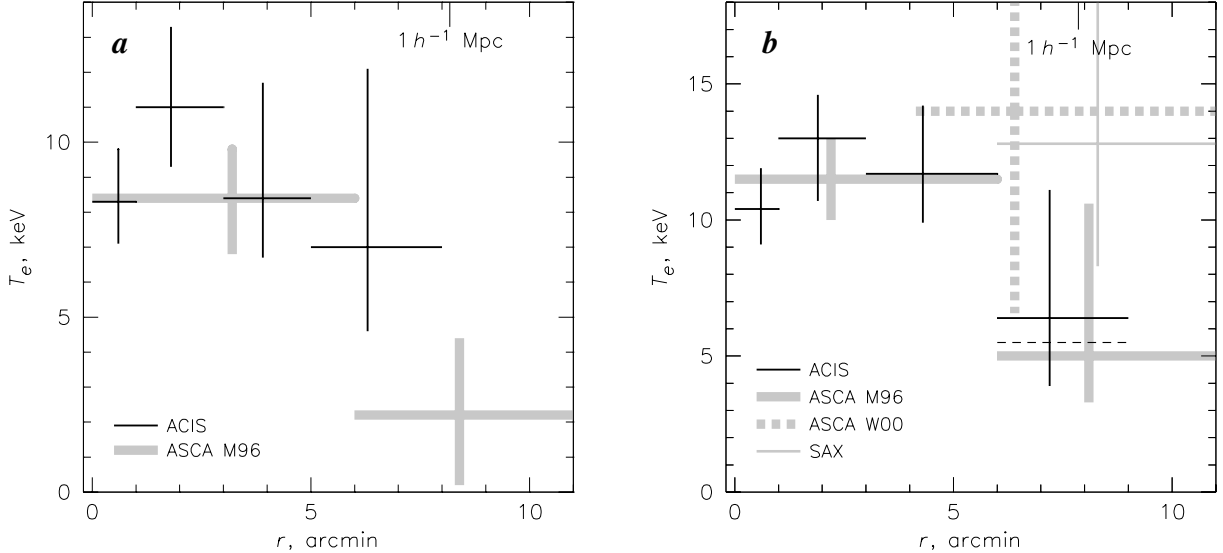


FIG. 2.—Radial projected temperature profiles, (a) for A665 and (b) for A2163. Black lines show results obtained here, while gray lines show earlier ASCA results from Markevitch (1996) and White (2000) and *BeppoSAX* results from Irwin & Bregman (2000). Uncertainties are 90% and crosses are centered at the emission-weighted radii. Black dashed line in panel (b) shows the best-fit temperature value with the soft background excess ignored (see text).

the CHIPY coordinate of the events, recalculating the PI values for the new coordinate, and normalizing the resulting images or spectra by the ratio of the readout exposure (41 ms) to the useful frame exposure (3.2 s).

2.2. Spectral fitting

To fit a spectrum in a large region, a telescope response file (ARF) was calculated by weighting the mirror effective area within the region with the observed cluster brightness distribution in the 0.5–2 keV band, taken as a representation of the cluster projected emission measure (the changes in vignetting within each region are negligible in this energy band). The spatial nonuniformity of the CCD quantum efficiency was also included in the ARF. For A665, observed at the focal plane temperature of -110°C when the CTI-induced nonuniformities were large, we used the formula by Vikhlinin (2000). For A2163, observed at -120°C which improved the uniformity, we used the standard QEU maps from the calibration database. The ARFs also included the position-independent, time-independent fudge factor of 0.93 at $E < 1.8$ keV to account for the flux discrepancy between the backside- and frontside-illuminated chips that characterizes the current (as of March 2001) combination of the spectral response matrices and quantum efficiency curves (Vikhlinin 2000). Response matrices (RMF) for each region were calculated by weighting the standard set of position-dependent matrices by the observed cluster brightness distribution within the region.

To fit the A665 spectra in large regions, we used the 0.8–9 keV energy band, while for A2163, the 1.2–10 keV band to minimize the background uncertainty (§2.1). A narrow interval around the mirror Ir edge (1.8–2.2 keV) was excluded due to the calibration inaccuracies causing significant residuals. Spectra were fit with the MEKAL model, fixing the absorption column to the Galactic value $N_H = 4.24 \times 10^{20} \text{ cm}^{-2}$ for A665 (Dickey & Lockman 1990) and to the *ROSAT* PSPC value $N_H = 1.65 \times 10^{21} \text{ cm}^{-2}$ for A2163 (Elbaz et al. 1995; this is slightly higher than the Galactic HI column $1.2 \times 10^{21} \text{ cm}^{-2}$). Freeing N_H resulted in best-fit values consistent with the above

assumptions. The background was modeled as described in §2.1. Changes of the best-fit temperature resulting from the $\pm 5\%$ change of the background normalization were added in quadrature to the statistical uncertainties of the temperatures to represent the 90% background uncertainty; it has noticeable effect only in the outer cluster regions.

2.3. Average temperatures

To check the consistency with earlier measurements, we first analyzed the spectra in $r = 6'$ regions that include most of the cluster emission. For A665, we obtain $T = 8.8 \pm 0.9$ keV, in agreement with the wide-aperture *Ginga* value (8.2 ± 0.9 keV, Birkinshaw, Hughes, & Arnaud 1991) and the ASCA value for the same $r = 6'$ region (8.4 ± 1.5 keV, Markevitch 1996). For A2163, we obtain $T = 12.3_{-1.1}^{+1.3}$ keV, marginally lower than the joint *Ginga* and *ROSAT* PSPC fit $14.6_{-0.8}^{+0.9}$ keV (Elbaz et al. 1995) and in agreement with the ASCA value for the same region (11.5 ± 1.5 keV, Markevitch 1996). We note here that without applying the correction to the ARFs at $E < 1.8$ keV mentioned above, the best-fit ACIS temperatures (10.5 keV for A665 and 15.2 keV for A2163) would be inconsistent with earlier results and the best-fit value of N_H for A2163 would be unreasonably high.

2.4. Temperature profiles

To derive the radial temperature profiles, we extracted the spectra in annuli centered on the cluster brightness peak (some of the annuli are incomplete due to the limited field of view). Point sources were excluded from the spectra. The fitting results are shown in Fig. 2. In general, the uncertainties are large due to the short exposures. For the outer region in A2163, we also show the temperature obtained by ignoring the soft background excess (black dashed line). The difference is within the uncertainty; for the inner annuli, it is unnoticeable.

For comparison, Figure 2 also includes earlier projected temperature profiles from ASCA (Markevitch 1996) that showed a temperature decline in both clusters. The Markevitch (1996)

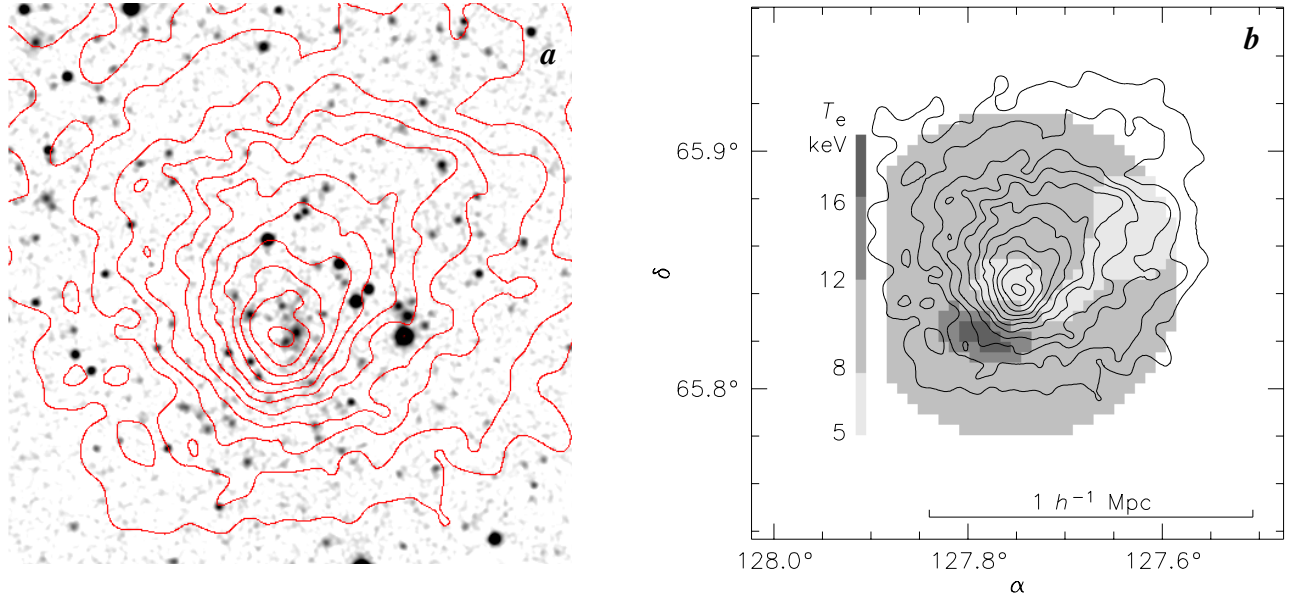


FIG. 3.—(a) A665 X-ray brightness contours (ACIS, 0.5–4 keV band) overlaid on the DSS plate. X-ray point sources were excluded before smoothing the image. The size of the DSS plate is $8.5'$ or $1.0\ h^{-1}$ Mpc. (b) ACIS temperature map (grayscale) overlaid on the X-ray contours. Different shades of gray approximately correspond to significantly different temperatures; contours are log-spaced by a factor $2^{1/2}$.

analysis was limited to $E > 2.5$ keV and therefore insensitive to the anomalous soft background in the A2163 field. An alternative ASCA derivation of the A2163 profile by White (2000) is also reproduced in Fig. 2b (only the interesting outer $r = 4' - 14'$ radial bin is shown for clarity).⁴ For A665, that work did not present measurements at the interesting off-center distances. For A2163, the last radial bin of the *BeppoSAX* profile from Irwin & Bregman (2000) is also shown. The new ACIS temperatures for A2163 are in agreement with the earlier values at all radii, except the Irwin & Bregman measurement that deviates by $\sim 2.4\sigma$. The new A665 profile does not cover the radii where the Markevitch (1996) ASCA fits showed the temperature drop. The new profile for A2163 does indicate a temperature decline at large radii, but the uncertainty is large. The forthcoming longer observation of A2163 with *Chandra* and the analysis of the *XMM* data (Pratt et al. 2001) will strengthen the constraints on the radial temperature decline in this interesting cluster.

2.5. Derivation of the temperature maps

Detailed temperature maps of the cluster central regions were derived by the technique described in Markevitch et al. (2000). For A665, we extracted images in the 0.7–2.5–5.0–9.0 keV bands, while for A2163, in the 0.8–2.5–4.5–8.0 keV bands (the number of energy intervals is limited by low statistics). Point sources were excluded. Background maps that included the genuine and the readout components (as described in §2.1) were subtracted from each image. The temperature maps are limited to the brightest regions of the clusters where the background accuracy is not as important as it is at large radii, thus to improve statistics, we chose to use a wider band for A2163 than that used for the profiles in §2.2. The images were then divided by the exposure maps that included vignetting and quantum efficiency nonuniformity (see §2.2). The resulting images were smoothed by a Gaussian filter with variable width, same for

all energy bands. A temperature in each pixel of the map was fitted using the data values from the smoothed images properly weighted with their errors, fixing N_H to the values given in §2.2. The resulting temperature maps, the first for A665 and A2163 with interesting spatial resolution, are discussed below.

3. DISCUSSION

Optical data for both clusters show significant structure, which may indicate either the genuine unrelaxed state or complex projection effects. In A665, Geller & Beers (1982) and Beers & Tonry (1986) noticed an elongation in galaxy number density distribution; on the other hand, Gómez, Hughes, & Birkinshaw (2000) detect “only subtle evidence for substructure” in the radial galactic velocities, suggesting that any merger activity should occur mostly in the plane of the sky. For A2163, the velocity data reveal significant subclustering in the redshift-coordinate space (Soucail, Arnaud, & Mathez in preparation). The X-ray data confirm that both clusters are mergers.

3.1. Merger in A665

The X-ray contours of A665 (Fig. 3a) are elongated in the same direction as the galaxy distribution (Geller & Beers 1982), and their appearance alone suggests that the bright core associated with the main galaxy concentration is flying in the southern direction with respect to the more diffuse cluster component (this was suggested, e.g., by Jones & Saunders 1996 already from the *ROSAT* PSPC image). Indeed, our ACIS temperature map, shown in Fig. 3b, reveals a remarkable shock in front of this flying core. The core itself is cooler than the cluster average. A less-apparent brightness elongation towards northwest is also cool; it likely corresponds to a remnant, and possibly a trail, of a smaller subcluster flying in the NW direction.

Examination of the ACIS images clearly shows that the excess hard emission at the position of the hot spot is extended.

⁴Their 1σ interval is converted to 90% and the cross is centered at the emission-weighted radius rather than the middle of the bin (at these radii, the cluster surface brightness declines with radius as r^{-4} , see, e.g., Vikhlinin et al. 1999). As seen from Fig. 2b, contrary to the impression that the White (2000) paper tried to convey, the two ASCA results did not disagree.

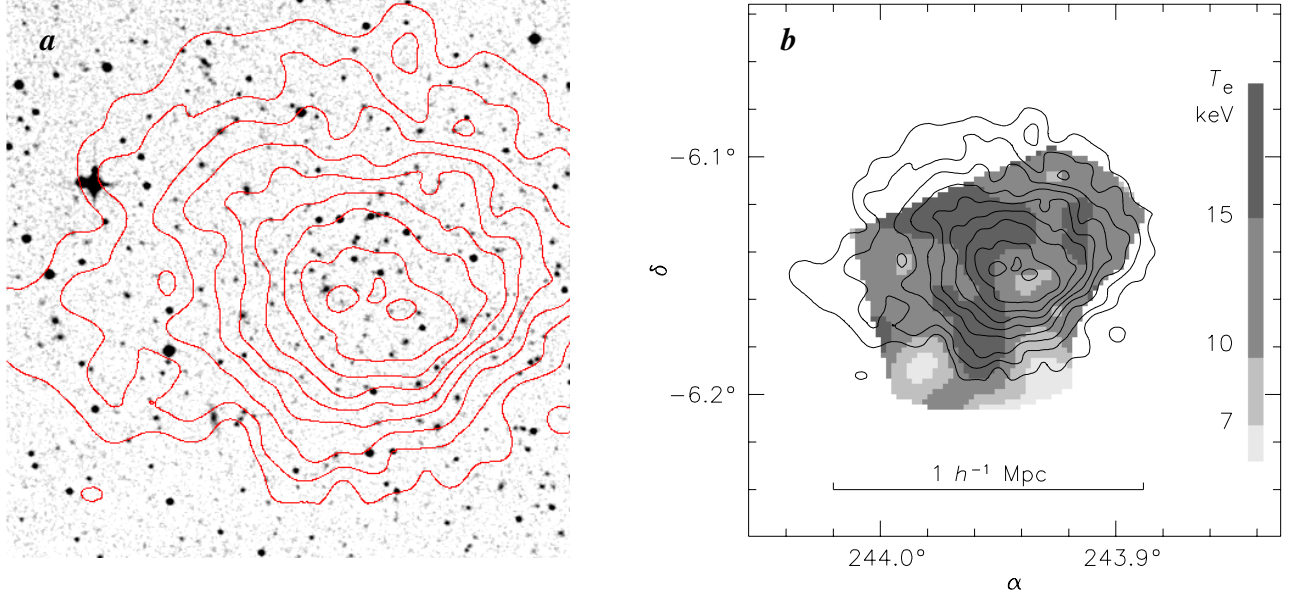


FIG. 4.—(a) A2163 X-ray brightness contours (ACIS, 0.8–4.5 keV band) overlaid on the DSS plate. The size of the DSS plate is $8.5'$ or $1.1 h^{-1}$ Mpc. X-ray point sources are excluded. (b) ACIS temperature map (grayscale) overlaid on the X-ray contours. Regions of the map with large relative uncertainties are cut off for clarity. Different shades of gray approximately correspond to significantly different temperatures. Contours are log-spaced by a factor $2^{1/2}$.

We have extracted a spectrum from the $0.7' \times 1.5'$ elliptical region centered on the hot spot. The fit gives a 90% lower limit of 15 keV; the value exceeds the average cluster temperature at the 98% confidence. Unfortunately, the number of photons from the hot region is insufficient to exclude a power-law component (the spectrum is fit equally well with a power law model with a photon index 1.0 ± 0.4). The possibility of a power-law inverse Compton contribution is discussed below (§3.4); here we can say that it cannot mimic the observed high temperature. If the hot region is a shock, it should be seen in the X-ray image as a gas density jump. The ACIS image does not show any sharp brightness edges either at the presumed bow shock or at the boundary of the cool core (such as those seen, e.g., in A3667 by Vikhlinin et al. 2001 or in 1E0657–56 by Markevitch et al. in preparation), although the image is not inconsistent with a more gradual density increase at the expected location. This can be naturally explained, for example, by projection effects due to a nonzero angle of the core velocity with respect to the plane of the sky.

To summarize, A665 appears to be at a stage when two cool subcluster remnants of very different sizes are flying apart after passing through each other (probably with a nonzero impact parameter, to explain the survival of both remnants). To some extent, this is similar to another merging cluster, A2142 (Markevitch et al. 2000), except that we do not see the sharp subcluster edges in A665 and do see a shock in the temperature map.

3.2. Merger in A2163

A *Chandra* image of A2163 is overlaid on the DSS plate in Fig. 4a. An obvious complex morphology of the image indicates that the cluster central region is in the state of violent motion. Neither of the three brightness peaks coincides with the maximum of the galactic density, and one can discern apparent streams of gas and asymmetric density gradients. As one can expect from the image, the temperature map is also complex

(Fig. 4b). The temperature varies by at least a factor of 2; there are two apparent shock regions coinciding with the gas density enhancements, while the central density peak is cool. To assess the statistical significance of these temperature deviations, we extracted spectra from three interesting regions, a $200'' \times 90''$ ellipse that includes the northern hot spot, an $r = 60''$ circle at the position of the southern hot spot, and an $r = 30''$ circle at the cool brightness peak. These spectra give $T > 17$ keV, $T > 16$ keV, and $T = 8.8^{+2.9}_{-1.8}$ keV (90% confidence), respectively; the first and the second hot spots deviate upwards from the cluster average by 3.4σ and 2.8σ , respectively, and the temperature at the center is below the average by 2σ , thus the gradients are significant. The northern hot spot was present, with a marginal significance, in the *ASCA* hardness ratio map (Markevitch et al. 1994); other features from that work are outside the area covered by the ACIS map. Preliminary *XMM* results (Bourdin 2001) appear to show similar temperature variations.

The structure in the A2163 temperature map is too complicated to try guessing a merger scenario (perhaps hydrodynamic simulations of the X-ray and optical data, as in, e.g., Roettiger et al. 1998 and 1999, would help). It appears that the density peak is a remnant of a cool subcluster that has survived a merger and is now surrounded by shock-heated gas.

3.3. Comparison with radio halos

Both A665 and A2163 have luminous radio halos (A665: Moffet & Birkinshaw 1989; Jones & Saunders 1996; Giovannini & Feretti 2000; A2163: Herbig & Birkinshaw 1994; Giovannini et al. 1999; Feretti et al. 2001). Having derived the gas temperature maps that reveal merger shocks, we can compare these maps to the radio halo images to determine whether the shocks indeed are the sites of the electron acceleration as proposed by Harris et al. (1980) and Tribble (1993).

Figures 5a and 6 show the 1.4 GHz radio halo images overlaid on the gas temperature maps. For A665, the radio image is reproduced from Giovannini & Feretti (2000). For A2163,

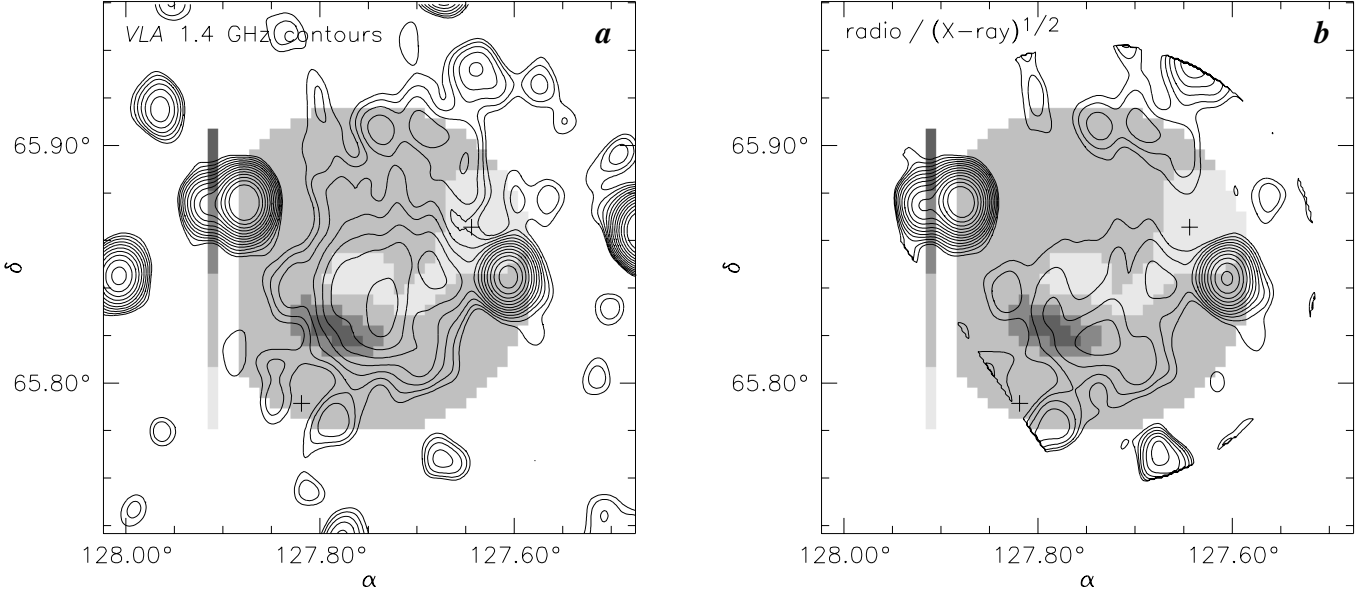


FIG. 5.—(a) A665 temperature map from Fig. 3 (grayscale) overlaid on the VLA 1.4 GHz contours of the radio halo from Giovannini & Feretti (2000). (b) Same as panel *a* but contours show radio brightness divided by square root of the X-ray brightness (edges are cut off for clarity). The two crosses indicate positions of the removed radio point sources; the angular resolution of the radio images is $45''$. Contours are log-spaced by a factor of $2^{1/2}$.

an image of the central bright region of the halo is retrieved from the public NVSS archive (this image was earlier presented in Giovannini et al. 1999). A new, higher-quality image has just been presented in Feretti et al. (2001) from which we took the positions of the point sources marked in Fig. 6. The old and new images are similar in their brightest regions.

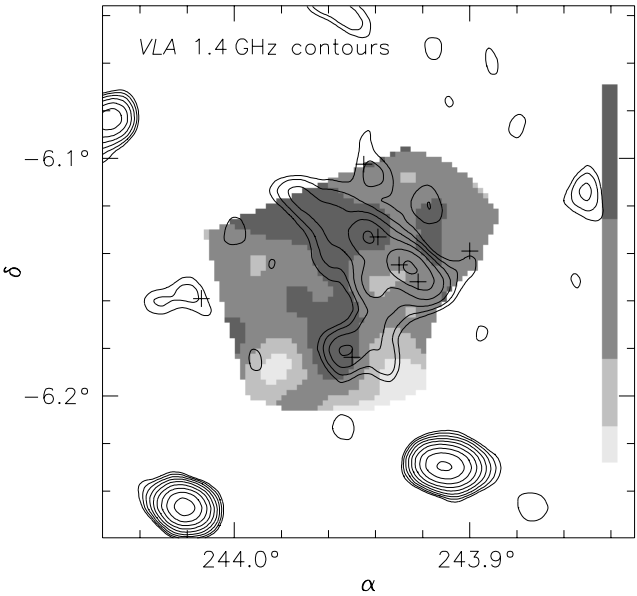


FIG. 6.—A2163 temperature map from Fig. 4 (grayscale) is overlaid on the VLA 1.4 GHz contours showing the central region of the radio halo (NVSS image, Giovannini et al. 1999). Contours are log-spaced by a factor of $2^{1/2}$. The angular resolution of the image is $45''$. Crosses (from Feretti et al. 2001) show positions of unrelated radio point sources in the central region.

In A665 (Fig. 5*a*), our X-ray shock region coincides with the distinct southeastern edge of the “limb-brightened” (Jones & Saunders 1996) radio halo, suggesting that this shock indeed plays a role in the generation of the halo. The overall geometry suggests that the large cool subcluster has arrived to the present location approximately from the northwest, with its shock blazing a trail of relativistic electrons along the way. These electrons are unlikely to penetrate the subcluster because of the disjoint magnetic field structure of the moving subcluster and the surrounding shock-heated gas, so in three dimensions, the trail would be hollow and produce the observed limb-brightened radio halo. (Some confusion is likely to be added by the subcluster moving at an angle to the sky plane as suggested in §3.1, so that most of the shock region would be projected onto the bright cool core where the X-ray-derived temperature is dominated by the core.) This qualitative scenario is not inconsistent with the Jones & Saunders’ estimate of an average age of the A665 halo, $t \lesssim 10^8$ yr. From the observed temperature jump across the shock (from $T_0 \approx 8$ keV to $T_1 > 15$ keV), the Mach number of the large subcluster is $M > 1.8$. A bow shock moving at 1.8–2.5 times the sound speed would travel of order $150 - 200 h^{-1}$ kpc during 10^8 yr, which is comparable to the size of the halo’s brightest region. An obvious observable prediction of this scenario would be that the radio spectrum of the halo at the present shock position would correspond to the youngest particles, while the “tail” of the halo would have a spectral signature of the old particles.

In A2163 (Fig. 6), there is also an apparent correlation between the gas temperature and the radio brightness — the main elongation of the halo’s brightest part coincides with the hottest region of the cluster (the southeastern radio elongation is apparently due to a point source). However, the hottest region itself coincides with an enhancement of the X-ray brightness (Fig. 4*b*). Feretti et al. (2001) report from a radio image with better sensitivity that on larger scales and at lower radio bright-

ness levels, the radio emission largely follows the X-ray emission. So for A2163, there is an ambiguity of whether the X-ray brightness or the gas temperature underlies the radio morphology. A similar observation of the large-scale similarity of the X-ray and radio brightness was made for several other clusters with well-studied halos (e.g., Deiss et al. 1997; Liang et al. 2000; Govoni et al. 2001).

However, for A665 with a more transparent merger geometry, it is clear that it is not simply the X-ray brightness, or the projected gas density, that determines the synchrotron brightness. Figure 5b shows the radio image divided by the square root of the X-ray brightness (to do this, we smoothed the X-ray image to the resolution of the radio image). A square root of an X-ray image crudely represents the projected distribution of the number density of thermal electrons. Therefore, such a ratio has an approximate physical meaning of the synchrotron brightness (or the number of relativistic electrons if the magnetic field is reasonably uniform) per thermal electron on the line of sight. As seen in Fig. 5b, this quantity peaks at the position of the shock. If the seed particles for acceleration are distributed more or less uniformly in the cluster thermal gas (as they are expected to be, for example, if the seeds come from the ICM pool as proposed by Liang et al. 2000), then the image of this ratio in A665 indicates that the particle acceleration indeed occurs at the shock site.

Several sources of the moderately high-energy seeds for acceleration to the ultra-relativistic energies were proposed (see, e.g., Enßlin 2000 for a review). Besides the high-energy tail of the ICM electrons and radio galaxies, they may include particles heated by mild turbulence induced by galaxy motions (e.g., Deiss et al. 1997) or past mergers. A discussion of these sources and the precise mechanism of acceleration is beyond the scope of this paper. Our results appear to indicate that in A665 and possibly in A2163, the final acceleration occurs inside the shock-heated gas. It is worth pointing out here that a merging cluster has to be in a favorable projection for a clear view of the shocks (as in A665), so one expects that in many clusters seen at less favorable angles, the temperature features and their association with the radio brightness would be less apparent.

3.4. Estimate of inverse Compton flux

The population of the relativistic electrons producing synchrotron radio halos should also scatter cosmic microwave background photons to X-ray energies via the inverse Compton (IC) mechanism. A tentative detection of the hard IC emission was reported for some clusters (Fusco-Femiano et al. 1999, 2000). One may ask whether the above correlation between the

temperature maps (which are, essentially, the X-ray hardness ratio maps) and the radio emission could be trivially explained by an IC contribution. The spectral index of the X-ray IC emission should be the same as the radio synchrotron index. Radio spectra of halos are steep; from the Jones & Saunders (1996) measurements at 1.4 GHz and 151 MHz, the energy index of the A665 halo is $\alpha_r \simeq 0.8$ (this is slightly less steep than a typical slope; they also present a higher frequency point where the spectrum steepens, but the lower frequencies are more relevant for the IC estimate). The expected IC spectrum ($\alpha_x = \alpha_r \simeq 0.8$) is much softer than the additional spectral component needed in our energy band to mimic the hot spot in A665 ($\alpha_x < 0$, which would require an unphysical power spectrum of the relativistic electrons). Thus the hot spot in A665 and, similarly, the hot regions in A2163, cannot be due to the IC contribution.

It is interesting to try and place a more accurate limit on the possible IC flux in the A665 hot spot region, since it is the place where the ratio of the radio to X-ray emission is highest. We can estimate the expected IC flux (as in, e.g., Sarazin 1988) using the estimates of the equipartition magnetic field and spectral index from Jones & Saunders (1996) and a 1.4 GHz flux from the Giovannini & Feretti (2000) radio map. The X-ray spectrum cannot exclude such a power-law component at a level up to two orders of magnitude above the expected flux. Thus, we cannot place interesting constraints on the IC contribution.

4. SUMMARY

Using *Chandra* data, we have derived gas temperature maps for the A665 and A2163 clusters. Both show strong temperature variations indicating ongoing mergers. In A665, we discover a bow shock in front of the cluster core indicating that the core is moving with a relatively high Mach number. In A2163, the temperature map is too complicated to allow unambiguous interpretation. Comparison with radio images shows that the hottest regions correlate with the brightest regions of the radio halos, indicating that acceleration of the relativistic electrons that generate the radio halos occurs at the sites of shock heating.

We are grateful to Leon VanSpeybroeck for allowing us to analyze his Guaranteed Time observations of A665 and A2163. We also thank him and Dan Harris for useful discussions, and Drs. G. Giovannini and L. Feretti for sending us their A665 radio image in electronic format. The results presented here are made possible by the successful effort of the entire *Chandra* team to build, launch and operate the observatory. Support for this study was provided by NASA contract NAS8-39073 and grant NAG5-9217.

REFERENCES

- Beers, T. C., & Tonry, J. L. 1986, *ApJ*, 300, 557
 Birkinshaw, M., Hughes, J. P., & Arnaud, K. A. 1991, *ApJ*, 379, 466
 Bourdin, H. 2001, talk at XXXVI Recontres de Moriond, March 10-17, Les Arcs, France
 Buote, D. A. 2001, *ApJ*, in press (astro-ph/0104211)
 Buote, D. A. & Tsai, J. C. 1996, *ApJ*, 458, 27
 Deiss, B. M., Reich, W., Lesch, H., & Wielebinski, R. 1997, *A&A*, 321, 55
 Dolag, K., & Enßlin, T. A. 2000, *A&A*, 362, 151
 Dickey, J. M., & Lockman, F. J. 1990, *ARA&A*, 28, 215
 Elbaz, D., Arnaud, M., & Böhringer, H. 1995, *A&A*, 293, 337
 Enßlin, T. A. 2000, in *The Universe at Low Radio Frequencies*, ASP Conference Series, in press (astro-ph/0001433)
 Feretti, L. 2000, in *The Universe at Low Radio Frequencies*, ASP Conference Series, in press (astro-ph/0006379)
 Feretti, L., Fusco-Femiano, R., Giovannini, G., & Govoni, F. 2001, *A&A*, in press (astro-ph/0104451)
 Fusco-Femiano, R., dal Fiume, D., Feretti, L., Giovannini, G., Grandi, P., Matt, G., Molendi, S., & Santangelo, A. 1999, *ApJ*, 513, L21
 Fusco-Femiano, R., et al. 2000, *ApJ*, 534, L7
 Geller, M. J., & Beers, T. C. 1982, *PASP*, 94, 421
 Gómez, P. L., Hughes, J. P., & Birkinshaw, M. 2000, *ApJ*, 540, 726
 Giovannini, G., & Feretti, L. 2000, *New Ast.*, 5, 335
 Govoni, F., Enßlin, T. A., Feretti, L., & Giovannini, G. 2001, *A&A* in press (astro-ph/010418)
 Giovannini, G., Tordi, M., & Feretti, L. 1999, *New Ast.*, 4, 141
 Harris, D. E., Kapahi, V. K., & Ekers, R. D. 1980, *A&AS*, 39, 215
 Henry, J. P., & Briel, U. G. 1995, *ApJ*, 443, L9
 Herbig, T., & Birkinshaw, M. 1994, American Astronomical Society Meeting, 185, 5307

- Irwin, J. A., & Bregman, J. N. 2000, *ApJ*, 538, 543
- Jaffe, W. J. 1977, *ApJ*, 212, 1
- Jones, M., & Saunders, R. 1996, Proc. Röntgenstrahlung from the Universe, 553 (MPE Report 263, eds. H. U. Zimmermann et al.)
- Kaastra, J. S. 1992, “An X-Ray Spectral Code for Optically Thin Plasmas” (Internal SRON-Leiden Report, updated version 2.0)
- Liang, H., Hunstead, R. W., Birkinshaw, M., & Andreani, P. 2000, *ApJ*, 544, 686
- Markevitch, M. 1996, *ApJ*, 465, L1
- Markevitch, M. 2001, *Chandra* calibration memo,
<http://asc.harvard.edu/cal/>, “ACIS”, “ACIS Background”
- Markevitch, M., et al. 2000, *ApJ*, 541, 542
- Markevitch, M., Sarazin, C. L., & Vikhlinin, A. 1999, *ApJ*, 521, 526
- Markevitch, M., Yamashita, K., Furuzawa, A., & Tawara, Y. 1994, *ApJ*, 436, L71
- Moffet, A. T., & Birkinshaw, M. 1989, *AJ*, 98, 1148
- Neumann, D. M., et al. 2001, *A&A*, 365, L74
- Pratt, G. 2001, talk at XXXVI Recontres de Moriond, March 10-17, Les Arcs, France
- Roettiger, K., Burns, J. O., & Stone, J. M. 1999, *ApJ*, 518, 603
- Roettiger, K., Stone, J. M., & Mushotzky, R. F. 1998, *ApJ*, 493, 62
- Sarazin, C. L. 1988, X-ray Emission from Clusters of Galaxies (Cambridge: Cambridge University Press)
- Tribble, P. 1993, *MNRAS*, 263, 31
- Vikhlinin, A. 2000, *Chandra* calibration memo,
http://asc.harvard.edu/cal/Links/Acis/acis/Cal_prods/qe/12_01_00
- Vikhlinin, A., Forman, W., & Jones, C. 1999, *ApJ*, 525, 47
- Vikhlinin, A., Markevitch, M., & Murray, S. S. 2001, *ApJ*, 551, 160
- White, D. A. 2000, *MNRAS*, 312, 663